Theoretical Studies of the sp^2 versus sp^3 C−H Bond Activation Chemistry of 2-Picoline by $(C_5Me_5)_2An(CH_3)_2$ Complexes (An = Th, U)

Ping Yang,* Ingolf Warnke,† Richard L. Martin, and P. Jeffrey Hay*

Los Alamos National Laboratory, Los Alamos, New Mexico 87545

Received September 18, 2007

The C−H bond activation chemistry of $(C_5Me_5)_2Th(CH_3)_2$ and $(C_5Me_5)_2U(CH_3)_2$ with 2-picoline (2-methylpyridine) is examined with use of density functional techniques. In particular, the differences between insertion into the ortho ring sp^2 C−H bond and the methyl sp^3 C−H bond are explored. The energies to form the η^2-(*N*,*C*)-pyridyl products resulting from the activation of the aromatic ring sp^2 C−H bond are calculated as thermodynamic products for both thorium and uranium systems with similar reaction energies of −15.8 kcal/mol. The products corresponding to insertion into the methyl sp^3 C−H bond are found to be higher in energy by 3.5 and 5.4 kcal/mol for Th and U, respectively. In the transition states the actinide atom mediates the hydrogen migration from 2-picoline to the leaving methyl group by forming an agostic five-centered C−H complex. The relative activation energies between sp^2 and sp^3 C−H bond activation differ slightly between Th, $\Delta E^{\ddagger}(sp^2) > \Delta E^{\ddagger}(sp^3)$ and U, $\Delta E^{\ddagger}(sp^2) < \Delta E^{\ddagger}(sp^3)$. These results are in agreement with the experimental observations that the sp^2 insertion product is the thermodynamic product in both cases, but that the sp^3 insertion product is the kinetic product in the case of Th.

Introduction

The thorium(IV) and uranium(IV) alkyl complexes $(C_5Me_5)_2AnR_2$ (where An = Th, U; R = CH_3, CH_2Ph, Ph) have proven to be versatile starting materials for the synthesis of a diverse array of actinide organometallic systems containing An−N bonds such as imido, hydrazonato, and ketimido complexes, which feature novel electronic properties.[1–5] It has been observed that complexes of lanthanide, actinide, and transition metal activate hydrocarbon substrates by different mechanisms.[6] Recently, Kiplinger and co-workers reported that these actinide alkyl complexes undergo interesting C−H and C−N bond cleavage chemistry with N-heterocycles. For example, the Th(IV) complexes $(C_5Me_5)_2Th(CH_3)_2$ and $(C_5Me_5)_2Th(CH_2Ph)_2$ readily react with the sp^2 C−H bonds in pyridine *N*-oxide and the sp^3 C−H bonds in 2,6-lutidine *N*-oxide, whereas the corresponding U(IV) complexes activate only the sp^2 C−H bonds in pyridine *N*-oxide (Scheme 1).[1]

Later studies[7,8] were carried out on 2-picoline (2-methylpyridine), which possesses both sp^2 and sp^3 hybridized C−H bonds. Deuterium labeling studies demonstrated that the thorium and uranium $(C_5Me_5)_2An(CH_3)_2$ complexes react with 2-picoline by different mechanistic reaction pathways. The thorium alkyl complex $(C_5Me_5)_2Th(CH_3)_2$ selectively activates a sp^3 C−H bond on the 2-picoline methyl group to give the kinetic α-picolyl product, $(C_5Me_5)_2Th(CH_3)[\eta^2$-(*N*,*C*)-2-$CH_2$-$NC_5H_3]$, which reacts with additional 2-picoline to afford the thermodynamic η^2-pyridyl product, $(C_5Me_5)_2Th(CH_3)[\eta^2$-(*N*,*C*)-6-$CH_3$-$NC_5H_3]$. This is in marked contrast with the uranium system that only reacts with a sp^2 C−H bond on the 2-picoline aromatic ring to give the η^2-pyridyl product $(C_5Me_5)_2U(CH_3)[\eta^2$-(*N*,*C*)-6-$CH_3$−$NC_5H_3]$, see Scheme 2. The deuterium-labeling studies suggested that the 2-picoline C−H activation chemistry is proceeded by σ-bond metathesis for both the thorium and uranium $(C_5Me_5)_2An(CH_3)_2$ complexes.[8]

Density functional theory (DFT) methods have been employed to explore actinide−ligand interactions in a variety of complexes, using the current generation of hybrid functionals. The structures, thermochemistry, and spectroscopic properties using such approaches provide information to compare with available structural and spectroscopic data.[9–16] By comparison,

* Corresponding authors. E-mail: pyang@lanl.gov; jeffhay@mywdo.com.
† Current address: Institut für Physikalische Chemie, Universität Karlsruhe (TH), Germany.

(1) Pool, J. A.; Scott, B. L.; Kiplinger, J. L. *J. Am. Chem. Soc.* **2005**, *127*, 1338–1339.
(2) Jantunen, K. C.; Burns, C. J.; Rodriguez, I. C.; Da Re, R. E.; Golden, J. T.; Morris, D. E.; Scott, B. L.; Taw, F. L.; Kiplinger, J. L. *Organometallics* **2004**, *23*, 4682.
(3) Kiplinger, J. L.; Morris, D. E.; Scott, B. L.; Burns, C. J. *Organometallics* **2002**, *21*, 3073.
(4) Wiedemann, S. H.; Lewis, J. C.; Ellman, J. A.; Bergman, R. G. *J. Am. Chem. Soc.* **2006**, *128*, 2452–2462.
(5) Bruno, J. W.; Smith, G. M.; Marks, T. J.; Fair, C. K.; Schultz, A. J.; Williams, J. M. *J. Am. Chem. Soc.* **1986**, *108*, 40–56.
(6) This field in transition metal has been extensively reviewed. For example: (a) Davies, J. A. W. P. L.; Liebman, J. F.; Greenberg, A., Eds. *Selective Hydrogencarbon Activation: Principles and Progress*; VCH Publishers: New York, 1990. (b) Arndtsen, B. A.; Bergman, G. G.; Mobley, T. A.; Peterson, T. H. *Acc. Chem. Res.* **1995**, *28*, 154–162. (c) Shilov, A. E.; Shul'pin, G. B. *Activation and Catalytic Reactions of Saturated Hydrocarbons in the Presence of Metal Complexes*; Kluwer: Boston, MA, 2000. (d) Crabtree, R. H. *J. Chem. Soc., Dalton Trans.* **2001**, 2437–2450. (e) Labinger, J. A.; Bercaw, J. E. *Nature* **2002**, *417*, 507–514. (f) Goldberg, K. I.; Goldman, A. S., Eds. *Activation and Functionalization of C-H Bonds*; ACS Symp. Ser. No. 885; American Chemical Society: Washington, DC, 2004, In.
(7) Pool, J. A.; Scott, B. L.; Kiplinger, J. L. *J. Alloys Compd.* **2006**, *418*, 178–183.
(8) Kiplinger, J. L.; Scott, B. L.; Schelter, E. J.; Pool Davis Tournear, J. A. *J. Alloys Compd.* **2007**, *444−445*, 477–482.
(9) Kaltsoyannis, N. *Chem. Soc. Rev.* **2003**, *32*, 9–16.
(10) Bursten, B. E.; Drummond, M. L.; Li, J. *Faraday Discuss.* **2003**, *124*, 1–24, 457–8.
(11) Clark, A. E.; Martin, R. L.; Hay, P. J.; Green, J. C.; Jantunen, K. C.; Kiplinger, J. L. *J. Phys. Chem. A* **2005**, *109*, 5481–5491.
(12) Peralta, J. E.; Batista, E. R.; Scuseria, G. E.; Martin, R. L. *J. Chem. Theory Comput.* **2005**, *1*, 612–616.
(13) Hayton, T. W.; Boncella, J. M.; Scott, B. L.; Palmer, P. D.; Batista, E. R.; Hay, P. J. *Science* **2006**, *310*, 1941–1943.
(14) Gagliardi, L.; Handy, N. C.; Ioanou, A. G.; Skylaris, C.-K.; Spencer, S.; Willetts, A.; Simper, A. M. *Chem. Phys. Lett.* **1998**, *283*, 187–193.

10.1021/om700927n CCC: $40.75
Publication on Web 03/13/2008

Scheme 1. $(C_5Me_5)_2Th(CH_3)_2$ and $(C_5Me_5)_2Th(CH_2Ph)_2$ Readily React with the sp^2 C−H Bonds in Pyridine *N*-Oxide and the sp^3 C−H Bonds in 2,6-Lutidine *N*-Oxide, whereas the Corresponding U(IV) Complexes Only Activate the sp^2 C−H Bonds in Pyridine *N*-Oxide

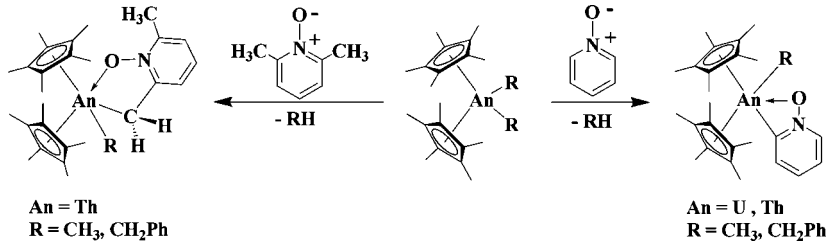

Scheme 2. The Thorium Alkyl Complex $(C_5Me_5)_2Th(CH_3)_2$ and 2-Picoline React To Give Preferential sp^3 C−H Bond Activation in the Presence of a More Reactive sp^2 C−H Bond, while the Analogous Uranium Complex, $(C_5Me_5)_2U(CH_3)_2$, Reacts with only the Ortho 2-Picoline sp^2 C−H Bond

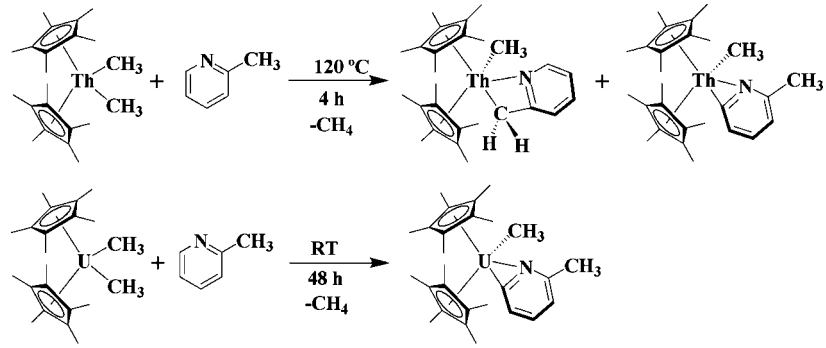

rather little information has been available on reaction mechanisms of f-element complexes such as in the aforementioned C−H activation processes. Most studies focus on the lanthanide compounds.[17–19] We have performed a computational study of the competitive sp^2 versus sp^3 C−H bond activation chemistry with 2-picoline and $(C_5Me_5)_2An(CH_3)_2$ for An and Th as shown in Scheme 2, where the competition between sp^2 and sp^3 C−H activations within the same reactant molecule is examined. Th(IV) complexes possess a closed shell electronic ground state ($5f^0$), while U(IV) systems represents a high-spin ($5f^2$) system with two unpaired electrons in f-orbitals.

The products and resulting thermochemistry in these reactions are compared for the cases of Th(IV) and U(IV), and likely reaction precursors and transition states are also identified. We find that the actinide atom plays a fundamental role during the hydrogen migration process from 2-picoline to the methyl leaving group. Agostic 5-centered transition structures for the actinide C−H activation reaction pathways are reported, to the best of our knowledge, for the first time.

Computational Details

The equilibrium molecular structures as well as transition state geometries of the actinide species involved in the C−H bond activation reactions were computed with use of density functional theory (DFT) techniques. The current approach chose a particular DFT method that gave excellent thermochemical predictions for actinide halide species[20,21] where there are available experimental quantities and applied it to the set of model Th and U reactions discussed above. Our calculations employed the hybrid B3LYP functional.[22,23] The Stuttgart RSC 1997 effective core potential (ECP) was used for the thorium and uranium atoms, where 60 core-electrons are replaced to account for scalar relativistic effects.[24] The valence electrons are represented by a contracted [8s/7p/6d/4f] basis; 6-31G* basis sets were used for carbon, hydrogen, and nitrogen. Spin–orbit interactions have not been considered explicitly. The effects of polarization functions on transition states were tested by reoptimizing the transition states by using the 6-31G** basis that contains p polarization functions on hydrogen atoms. The newly found transition states were essentially identical structurally with the ones found by using the 6-31G* basis sets, and thermochemistry and reaction barriers differed by less than 0.5 kcal. Harmonic vibrational analyses were performed to confirm that structures were minima or saddle points and to obtain the thermochemical corrections to the energy, entropy, and Gibbs free energy. Inclusion of these effects results in changes of ∼1 kcal/mol in reaction energies and leads to the same relative ordering (see the Supporting Information). All thermodynamic data were calculated at the standard state (298.15 K and 1 atm). The intrinsic reaction coordinate (IRC) method was used to follow the reaction path in

(15) Gagliardi, L.; Schimmelpfennig, B.; Maron, L.; Wahlgren, U.; Willetts, A. *Chem. Phys. Lett.* **2001**, *344*, 207–212.

(16) Kaltsoyannis N.; Hay, P. J.; Li, J ; Blaudeau, J. P.; Bursten, B. E. Theoretical Studies of the Electronic Structure of Compounds of the Actinide Elements. In *The Chemistry of the Actinide and Tranactinide Elements*, 3rd ed.; Morss, L. R., Edelstein, N. M., Fuger, J., Eds.; Springer: Dordrecht, The Netherlands, 2006; Vol. 3.

(17) Sherer, E. C.; Cramer, C. J. *Organometallics* **2003**, *22* (8), 1682–1689.

(18) Barros, N.; Eisenstein, O.; Maron, L. *Dalton Trans.* **2006**, (25), 3052–3057.

(19) de Almeida, K. J.; Cesar, A. *Organometallics* **2006**, *25*, 3407–3416.

(20) Batista, E. R.; Martin, R. L.; Hay, P. J. *J. Chem. Phys.* **2004**, *121*, 11104–11111.

(21) Batista, E. R.; Martin, R. L.; Peralta, J. E.; Scuseria, G. E. *J. Chem. Phys.* **2004**, *121*, 2144–2150.

(22) Becke, A. D. *J. Chem. Phys.* **1993**, *98*, 5648.

(23) We also tested a few functionals on the relative energies. Since the geometries are not sensitive to the functional used, the single point energy difference was compared between thorium transition states $\mathbf{TS_{5A\text{-}2A}}$ (sp^3) and $\mathbf{TS_{5A\text{-}1A}}$ (sp^2): −0.54 kcal/mol for B3LYP, −0.71 kcal/mol for B3PW91, −1.42 kcal/mol for TPSS, and −1.92 kcal/mol for BMK. The chosen functional B3LYP described the essential properties and fundamental chemistry of these compounds but slightly underestimated the energy difference compared to others.

(24) Dolg, M.; Stoll, H.; Preuss, H.; Pitzer, R. M. *J. Phys. Chem.* **1993**, *97*, 5852.

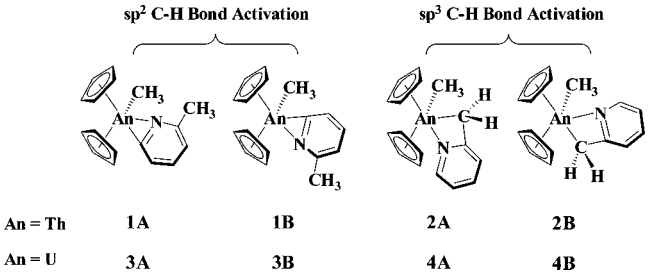

Figure 1. Possible isomers of the products resulting from the C−H bond activation chemistry between $(C_5H_5)_2An(CH_3)_2$ (An = Th, U) and 2-picoline. These isomers are labeled as **1A***, **1B***, **2A***, **2B***, **3A***, **3B***, **4A***, and **4B*** when the ligands are Cp*, i.e., $(C_5Me_5)_2An(CH_3)_2$ (An = Th, U).

both directions from the transition state.[25,26] Solvation effects were investigated by using polarizable continuum models (PCM) in the solvent toluene ($\epsilon = 2.38$) employing UFF atomic radii.[27,28] All calculations were carried out with the Gaussian03 suite of codes.[29] Analysis of the electronic structure was carried out using the Natural Bond Orbital (NBO) approach.[30]

Results and Discussion

In the following sections the DFT results are presented for the species involved in the reactions of the thorium and uranium $(C_5Me_5)_2An(CH_3)_2$ complexes shown in Scheme 2. First, the structures and thermochemistries of the two classes of products arising from sp^2 and sp^3 C−H bond activation are examined for both C_5Me_5 and model C_5H_5 ligands. These results help to focus the subsequent study of reaction pathways in which only C_5H_5 ligands were employed. In the second step, adducts of the actinide complexes with 2-picoline were examined as precursors for the reactions. Transition states from these adducts to the products were then identified and characterized theoretically, followed by reaction pathway analyses. Finally, the electronic properties of all these species are analyzed.

Products from Competitive sp^2 versus sp^3 C−H Bond Activation Chemistry. Structures. The geometries of all possible products for the thorium and uranium sp^2 and sp^3 C−H bond activation reactions were fully optimized. Both the Cp* (C_5Me_5 or pentamethylcyclopentadienyl) compounds and simplified model Cp (C_5H_5 or cyclopentadienyl) complexes were examined. As illustrated in Figure 1, there are four possible

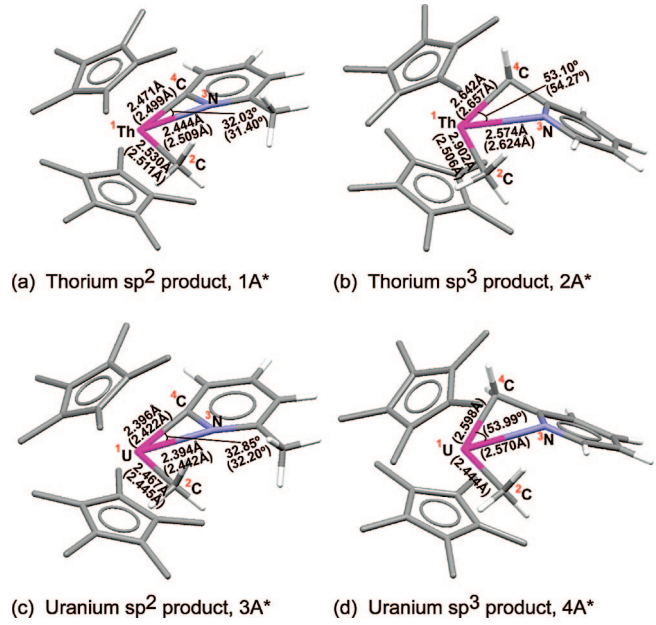

Figure 2. The calculated 3D structures for the possible sp^2 and sp^3 C−H bond activation products. The geometric data obtained from crystal structures (from ref 8) are shown above the calculated data, which are in parentheses. The bond lengths are given in angstroms and bond angles are given in degrees.

products for the C−H activation chemistry of $(C_5Me_5)_2Th(CH_3)_2$ with 2-picoline. Two isomers result from activation of the sp^2 C−H bond ortho to the ring nitrogen atom, $(C_5Me_5)_2Th(CH_3)\eta^2$-(*N*,*C*)-6-Me-$NC_5H_3$] (**1A*** and **1B***). Two additional possibilities arise from activation of the sp^3 C−H bond on the 2-picoline methyl group, which depend on the orientation of the methyl group giving $(C_5Me_5)_2Th(CH_3)\eta^2$-(*N*,*C*)-2-$CH_2$−$NC_5H_4$] (**2A*** and **2B***). We refer to the analogous species for the Cp ligand by omitting the asterisk as simply **1A**, **1B**, etc.

The optimized ground-state geometries are presented in Figure 2 and Tables 1 and 2. Table 1 compares the geometric data for the thorium products obtained from available crystal structures with those data calculated for both Cp* and Cp complexes. Table 2 shows the corresponding geometric data for uranium complexes. Figure 3 illustrates the numbering and labeling scheme employed for the following discussions regarding the calculated adduct, transition state, and product structures. Excellent agreement is obtained between the experimental and calculated structures, with An−C bond lengths deviating by 0.05 Å and the bond angles deviating by 3°. The largest variation is observed for the An−N bond lengths, with deviations of only 0.05 Å. We need to point out that the only discrepancy is the Th^1-C^2 bond length of the methyl group bound to the Th in the sp^3 product. In this case the experimental bond length (2.902 Å) is well out of the normal range of thorium carbon single bond lengths of about 2.5 Å. Aside from this one exception, considering that the calculations are for gas-phase geometries and the X-ray crystal data are for solid-state geometries, the agreement between the two is quite remarkable.

The Th^1-C^2 bond lengths in the products are slightly lengthened (~0.02 Å) compared to the $Th-C_{methyl}$ bond distance of 2.483 Å calculated for the starting material model complex $(C_5H_5)_2ThMe_2$. This result is not too surprising since the small methyl group is being replaced by the more bulky picolyl ligand. The insertion of the picolyl group also causes the angles between the two C_5H_5 rings to increase marginally by 2–5°. The bent-metallocene framework of the reactant does not change and both

(25) Gonzalez, C.; Schlegel, H. B. *J. Chem. Phys.* **1989**, *90*, 2154.
(26) Gonzalez, C.; Schlegel, H. B. *J. Phys. Chem.* **1990**, *94*, 5523.
(27) Miertus, S.; Scrocco, E.; Tomasi, J. *Chem. Phys.* **1981**, *55*, 117.
(28) Cammi, R.; Mennucci, B.; Tomasi, J. *J. Phys. Chem. A* **2000**, *104*, 5631.
(29) Frisch, M. J.; Trucks, G. W.; Schlegel, H. B.; Scuseria, G. E.; Robb, M. A.; Cheeseman, J. R.; Montgomery, J. A.; Vreven, J. T.; Kudin, K. N.; Burant, J. C.; Millam, J. M.; Iyengar, S. S.; Tomasi, J.; Barone, V.; Mennucci, B.; Cossi, M.; Scalmani, G.; Rega, N.; Petersson, G. A.; Nakatsuji, H.; Hada, M.; Ehara, M.; Toyota, K.; Fukuda, R.; Hasegawa, J.; Ishida, M.; Nakajima, T.; Honda, Y.; Kitao, O.; Nakai, H.; Klene, M.; Li, X.; Knox, J. E.; Hratchian, J. P.; Cross, J. B.; Adamo, C.; Jaramillo, J.; Gomperts, R.; Stratmann, R. E.; Yazyev, O.; Austin, A. J.; Cammi, R.; Pomelli, C.; Ochterski, J. W.; Ayala, P. Y.; Morokuma, K.; Voth, G. A.; Salvador, P.; Dannenberg, J. J.; Zakrzewski, V. G.; Dapprich, S.; Daniels, A. D.; Strain, M. C.; Farkas, O.; Malick, D. K.; Rabuck, A. D.; Raghavachari, K.; Foresman, J. B.; Ortiz, J. V.; Cui, Q.; Baboul, A. G.; Clifford, S.; Cioslowski, J.; Stefanov, B. B.; Liu, G.; Liashenko, A.; Piskorz, P.; Komaromi, I.; Martin, R. L.; Fox, D. J.; Keith, T.; Al-Laham, M. A.; Peng, C. Y.; Nanayakkara, A.; Challacombe, M.; Gill, P. M. W.; Johnson, B.; Chen, W.; Wong, M. W.; Gonzalez, C.; Pople, J. A. *Gaussian03*, Revision C.02; Gaussian, Inc.: Wallingford, CT, 2004.
(30) Glendening, E. D.; Badenhoop, J., K.; Reed, A. E.; Carpenter, J. E.; Bohmann, J. A.; Morales, C. M.; Weinhold, F. *NBO 5.0*; Theoretical Chemistry Institute, Univeristy of Wisconsin: Madison, WI, 2001.

Table 1. Experimental Data Obtained from Crystal Structures and Calculated Structural Data for the Possible Products Resulting from sp^2 and sp^3 C−H Bond Activation Chemistry between $(C_5Me_5)_2Th(CH_3)_2$ and 2-Picoline

	reactant	sp^2 products			sp^3 products		
	$Cp^*_2ThMe_2(Cp_2ThMe_2)$	exptl[8] **1A***	calcd **1A*** (**1A**)	calcd **1B*** (**1B**)	exptl[8] **2A***	calcd **2A*** (**2A**)	calcd**2B*** (**2B**)
$R(Th^1-C^2)^a$	2.489[b] (2.483)[c]	2.530	2.511 (2.507)	2.497 (2.494)	2.902	2.506 (2.508)	2.491 (2.496)
$R(Th^1-N^3)^a$		2.444	2.509 (2.497)	2.544 (2.505)	2.574	2.624 (2.599)	2.661 (2.585)
$R(Th^1-C^4)^a$		2.471	2.499 (2.498)	2.496 (2.496)	2.642	2.657 (2.660)	2.640 (2.668)
$\angle(N^3-Th^1-C^4)^a$		32.03°	31.40° (31.52°)	31.26° (31.53°)	53.10°	54.27° (53.06°)	52.72° (53.15°)

[a] The labeling scheme is shown in Figure 3, and is adopted by Tables 2−6. [b] The experimental and optimized geometric parameters with C_5Me_5 ligands (**1A***, **1B***, **2A***, **2B***) are shown. [c] The optimized geometric parameter with C_5H_5 ligands (**1A**, **1B**, **2A**, **2B**) are shown in parentheses.

Table 2. Experimental Data Obtained from Crystal Structures and Calculated Structural Data for the Possible Products Resulting from sp^2 and sp^3 C−H Bond Activation Chemistry between $(C_5Me_5)_2U(CH_3)_2$ and 2-Picoline

	reactant	sp^2 products			sp^3 products	
	$Cp^*_2UMe_2(Cp_2UMe_2)$	exptl[8] **3A***	calcd **3A*** (**3A**)	calcd. **3B*** (**3B**)	calcd **4A*** (**4A**)	calcd **4B*** (**4B**)
$R(U^1-C^2)^a$	2.418[b] (2.406)[c]	2.467	2.445 (2.439)	2.428 (2.414)	2.444 (2.441)	2.423 (2.429)
$R(U^1-N^3)^a$		2.394	2.442 (2.428)	2.481 (2.453)	2.570 (2.524)	2.677 (2.552)
$R(U^1-C^4)^a$		2.396	2.422 (2.423)	2.408 (2.412)	2.598 (2.609)	2.540 (2.579)
$\angle(N^3-U^1-C^4)^a$		32.85°	32.20° (32.32°)	32.04° (32.22°)	53.99° (54.29°)	53.45° (54.38°)

[a] The labeling scheme is shown in Figure 3, and is adopted by Tables 2−6. [b] The experimental and optimized geometric parameters with C_5Me_5 ligands (**1A***, **1B***, **2A***, **2B***) are shown. [c] The optimized geometric parameter with C_5H_5 ligands (**1A**, **1B**, **2A**, **2B**) are shown in parentheses.

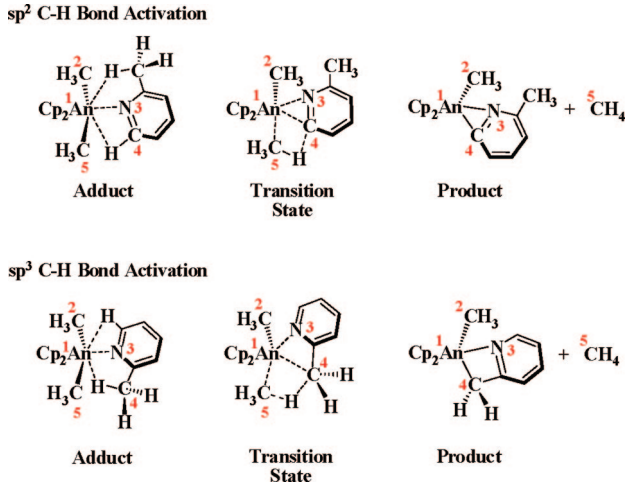

Figure 3. The labeling scheme for calculated adducts, transition states, and products in the sp^2 and sp^3 C−H bond activation chemistry between $(C_5H_5)_2An(CH_3)_2$ (An = Th, U) and 2-picoline. In particular, the structures along the reaction pathways for products A series are shown as examples.

Table 3. Summary of the Calculated Binding Energies (all values in kcal/mol) for the Possible Adducts and Reaction Energies Relative to the Sum of Reactants for the C−H Bond Activation Chemistry between 2-Picoline and $(C_5Me_5)_2An(CH_3)_2$ or $(C_5H_5)_2An(CH_3)_2$ (An = Th, U)

	Th		U	
	complex	energy	complex	energy
product (C_5Me_5)	**1A***	−15.81	**3A***	−15.71
	1B*	−12.89	**3B***	−12.60
	2A*	−12.47	**4A***	−10.35
	2B*	−10.11	**4B***	−7.74
product (C_5H_5)	**1A**	−18.25	**3A**	−17.70
	1B	−16.25	**3B**	−16.85
	2A	−16.58	**4A**	−15.44
	2B	−15.32	**4B**	−14.70
adduct (C_5H_5)	**5A**	−1.80	**6A**	−0.16
	5B	0.40	**6B**	0.86
	5C	0.25	**6C**	1.40
	5D	4.72	**6D**	10.94

ligands stay within the metallocene wedge. The sp^2 C−H bond activation products (**1A** and **1B**) are η^2-(*N*,*C*)-pyridyl complexes with the actinide atom lying in the plane of the coordinated picolyl ligand. On the other hand, the sp^3 C−H bond activation products (**2A** and **2B**) have a bent configuration with the actinide center being folded out of the pyridine ring plane. The calculated structures for the uranium products are essentially identical with the thorium complexes with slightly shorter bond lengths, which is consistent with the contraction of ionic radius as one proceeds down the actinide series.

In general, the model C_5H_5 complexes perform well in reproducing the geometric parameters of the C_5Me_5 complexes, including reactants and products for both the observed thorium and uranium chemistry. The bonds for the coordinated picolyl and methyl ligands in the model C_5H_5 complexes are identical with the C_5Me_5 structures with bond lengths within 0.02 Å and bond angles within 2°. These errors are within the errors of experimental measurement. The only noticeable difference is the plane angle between the two C_5H_5 rings, which is about 10 larger than that observed for the more sterically congested bis(pentamethylcyclopentadienyl) system. These results are provided in tables in the Supporting Information.

Thermochemistry. The computed reaction energies showing the relative stability of the products for the two insertion pathways for Th and U complexes are given in Table 3 and Figure 4. Results are given for both the model C_5H_5 complexes as well as the C_5Me_5 complexes studied experimentally. As shown in Table 3, the reaction energies are exothermic in all cases and range from −14.70 to −18.25 kcal/mol for the model C_5H_5 complexes and from −7.74 to −15.81 kcal/mol for the C_5Me_5 complexes. The reaction energies for the sp^2 and sp^3 C−H bond activation pathways corresponding to the lowest isomer for the thorium and uranium complexes are plotted in

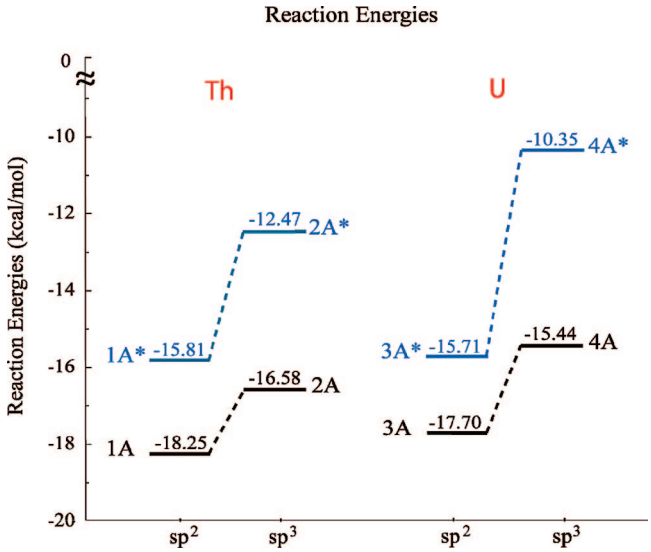

Figure 4. Reaction energies calculated for the sp^2 and sp^3 C−H bond activation products from the reaction between $(C_5Me_5)_2An(CH_3)_2$ or $(C_5H_5)_2An(CH_3)_2$ (An = Th, U) and 2-picoline. The numbers on bars are the reaction energies for corresponding compounds.

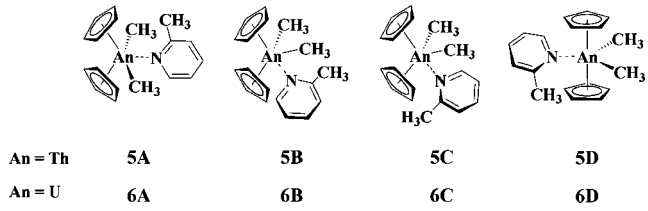

Figure 5. The possible adducts involved along the reaction pathways in the sp^2 and sp^3 C−H bond activation chemistry between $(C_5H_5)_2An(CH_3)_2$ (An = Th, U) and 2-picoline.

the Figure 4 for both C_5Me_5 and C_5H_5 ligand frameworks. The product **1A*** corresponding to the Th sp^2 C−H bond activation product is the most stable structure among all four products considered. It lies 3.34 kcal/mol lower in energy than the isomer **2A*** corresponding to the sp^3 C−H bond activation product. The same ordering is obtained for the thorium model C_5H_5 complexes, where **1A** is 1.67 kcal/mol lower in energy than **2A**.

For the uranium C_5Me_5 complexes, the same trend is observed with **3A*** being more stable in energy than **4A*** by 5.36 kcal/mol. For the C_5H_5 model compounds, **3A** is 2.26 kcal/mol lower in energy than **4A**. The energy difference between two products for uranium is larger than that for thorium (Table 3). Overall, these results are consistent with the experimental observations in that the sp^2 C−H bond activation products (**1A*** and **3A***) are the thermodynamically stable products. Since the same trends in reaction energies are reproduced by the model C_5H_5 ligands, the reaction pathways examined in later sections have employed C_5H_5 ligands. Geometrical analysis regarding the differences between the possible products provides insight into the regioselectivity observed for these reactions. As illustrated in Figure 1, for the thorium complexes, other possible products are **1B*** and **2B***, but each is less stable than **1A*** and **2A*** by 2.92 and 2.36 kcal/mol, respectively. These numbers reduce to 2.00 and 1.26 kcal/mol for the model C_5H_5 complexes. In comparison to **1A***, **1B*** has longer bond distances of Th−N and average Th−C to Cp rings, but a shorter Th−C bond length. This is likely due to steric interactions introduced by the orientation of the exo methyl group on the picolyl ligand. The picolyl methyl group encounters unfavorable steric interaction with the methyl groups on C_5Me_5 ligands resulting in greater congestion and a higher energy configuration. For the uranium complexes, the relative differences between the alternate products mirror their thorium counterparts, with **1B*** and **2B*** higher by 3.11 and 2.61 kcal/mol compared to **3A*** and **4A***, respectively. These

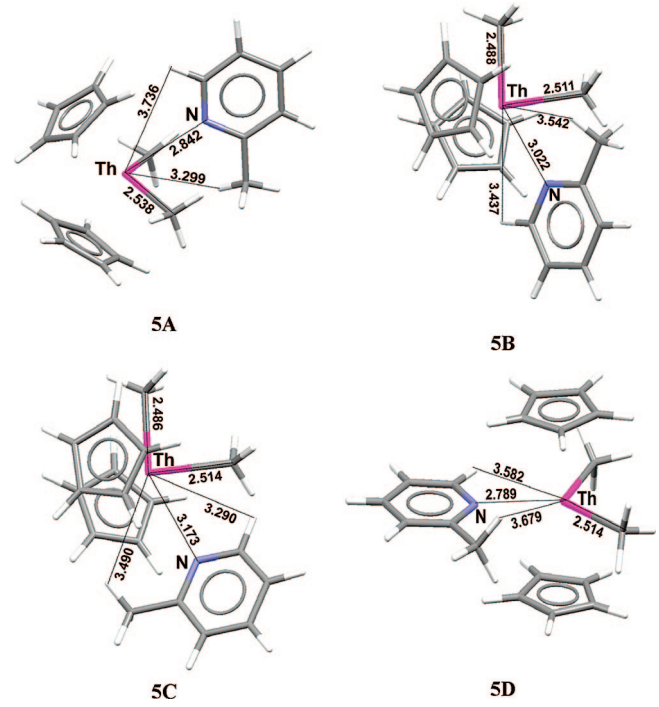

Figure 6. The calculated 3D structures for the possible adducts involved in the C−H bond activation chemistry between $(C_5H_5)_2Th(CH_3)_2$ and 2-picoline.

Table 4. Calculated Geometric Parameters for 2-Picoline Adducts with $(C_5H_5)_2An(CH_3)_2$ (An = Th, U)

	Th		U	
geometry	**5A**	**5D**	**6A**	**6D**
$R(An^1-C^2)$	2.538	2.514	2.476	2.469
$R(An^1-C^5)$	2.538	2.514	2.476	2.471
$R(An^1-N^3)$	2.842	2.789	2.778	2.728
$R(An^1-H(sp^2))$	3.736	3.582	3.455	3.469
$R(An^1-H(sp^3))$	3.299	3.679	3.401	3.633
$R_{avg}(An^1-C_{Cp1})$	2.871	2.904	2.805	2.844
$R_{avg}(An^1-C_{Cp2})$	2.857	2.909	2.791	2.850
D(Cp1−Cp2)	66.20°	4.43°	60.80°	4.45°

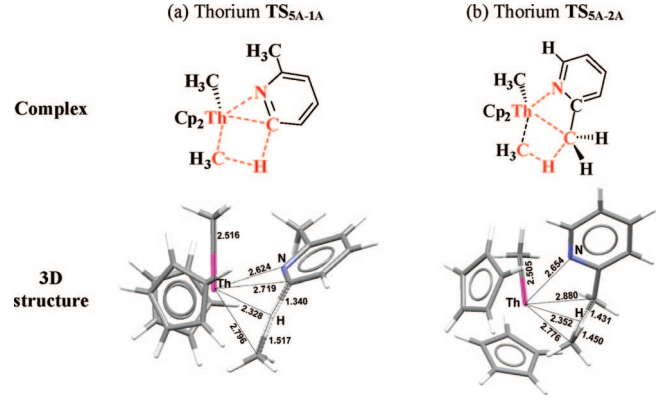

Figure 7. The calculated 3D structures of the transition states involved in the sp^2 and sp^3 C−H bond activation of 2-picoline from the thorium adduct **5A**.

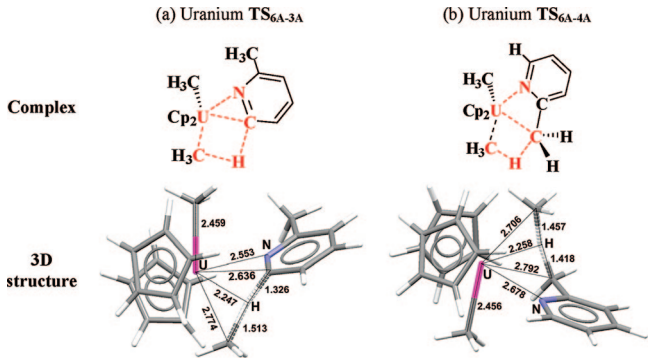

Figure 8. The calculated 3D structures of the transition states involved in the sp^2 and sp^3 C−H bond activation of 2-picoline from the uranium adduct **6A**.

Table 5. Metrical Data from the Calculated Transition States Structures for the sp^2 and sp^3 C−H Bond Activation Chemistry between $(C_5Me_5)_2An(CH_3)_2$ (An = Th, U) and 2-Picoline

metrical parameter	Th		U	
	sp^2 **TS5A-1A**	sp^3 **TS5A-2A**	sp^2 **TS6A-3A**	sp^3 **TS6A-4A**
$R(An^1-C^2)$	2.516	2.505	2.459	2.456
$R(An^1-H)$	2.328	2.352	2.247	2.258
$R(An^1-N^3)$	2.264	2.654	2.553	2.678
$R(An^1-C^4)$	2.719	2.880	2.636	2.792
$R(An^1-C^5)$	2.796	2.776	2.774	2.706
$R_{avg}(An^1-C_{Cp1})$	2.852	2.891	2.787	2.816
$R_{avg}(An^1-C_{Cp2})$	2.860	2.878	2.792	2.792
$\angle(N^3-An^1-C^4)$	29.25°	50.62°	30.04°	50.84°
$\angle(N^3-An^1-C^2)$	74.36°	75.23°	76.08°	74.48°
$\angle(C^2-An^1-C^4)$	85.56°	83.15°	94.68°	86.59°
D(Cp1−Cp2)	58.64°	63.15°	58.70°	63.25°

numbers reduce to 0.85 and 0.74 kcal/mol for the C_5H_5 systems. Overall, the model C_5H_5 systems accurately reflect the relative thermochemical relationships among the C_5Me_5 products, but with smaller energy difference.

Adducts of $(C_5H_5)_2An(CH_3)_2$ (An = Th, U) with 2-Picoline. Although the existence of stable adducts is not required along reaction paths leading to C−H bond activation, the possible 2-picoline adducts with the model complexes $(C_5H_5)_2An(CH_3)_2$ (An = Th, U) were examined to gain mechanistic insights into the C−H bond activation reaction processes as well as to aid in the identification of transition states for the C−H activation reactions. As illustrated in Figure 5, the 2-picoline ligand can approach the metal center in one of three ways, leading to four possible adduct structures:

(1) A frontal approach between two methyl groups. There are two possible orientations for the 2-picoline ring relative to the plane formed by the actinide metal center and the carbon atoms on two methyl groups, parallel or perpendicular. The perpendicular conformation is preferred (**5A** and **6A**), while the parallel configuration is unstable due to large unfavorable steric interactions between the 2-picoline methyl group and the actinide methyl groups.

(2) A lateral approach from the side of the metallocene. In this case, two stable conformations can also be formed as a result of different orientations of the 2-picoline methyl group. Adducts **5B** and **6B** are formed when the 2-picoline methyl group is pointing toward the actinide methyl groups and complexes **5C** and **6C** have the 2-picoline methyl group directed away from the actinide methyl groups.

(3) A backside approach of the 2-picoline forming the linear metallocene complexes **5D** and **6D** with the two C_5H_5 rings being parallel.

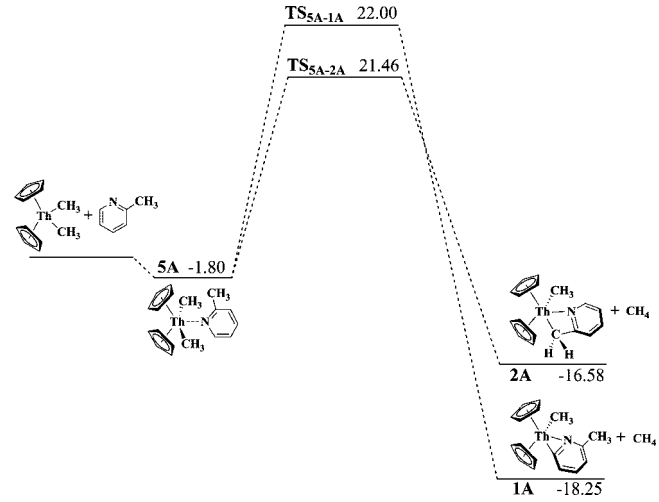

Figure 9. Reaction energy diagram for the sp^2 and sp^3 C−H bond activation chemistry between $(C_5H_5)_2Th(CH_3)_2$ and 2-picoline.

Table 6. Activation Energies (all values are in kcal/mol) Relative to the Sum of Reactants

	Th		U	
	complex	energy	complex	energy
sp^2 TS	**TS5A-1A**	22.00	**TS6A-3A**	21.57
	TS5C-1B	24.90	**TS6C-3B**	27.20
	TS5D-1A	34.42	**TS6D-3A**	21.62
sp^3 TS	**TS5A-2A**	21.46	**TS6A-4A**	22.80
	TS5B-2B	24.94	**TS6B-4B**	28.38
	TS5D-2A	35.49	**TS6D-4A**	22.79

The optimized three-dimensional structures of the possible adducts for thorium (**5A**−**D**), all of which are local minima, are shown in Figure 6. The summarized geometric parameters for the thorium 2-picoline adducts **5A** and **5D** and the uranium 2-picoline adducts **6A** and **6D** are presented in Table 4. For both thorium and uranium systems, the most stable adducts are **5A** and **6A**, respectively, which are the only adducts calculated to be exothermic relative to the $(C_5H_5)_2An(CH_3)_2$ and 2-picoline reactants.

For all the calculated adducts, the An^1-N^3 distances are in the range of 2.8–3.2 Å, which are longer than the An−N distances of the products. The coordination interactions for these adducts are fairly weak resulting in very small binding energies and slightly longer (by 0.05 Å) An^1-C^2 bond lengths. The distances between the actinide metal center and the *o*-H ($An\cdots H-C_{sp^2}$) and the closest H atom on the methyl group ($An\cdots H-C_{sp^3}$) on the coordinated 2-picoline are in the range of 3.3–3.7 Å. Therefore, no substantial interactions exist between the actinide center and these hydrogen atoms in the adduct structures.

However, it is worth pointing out that for the most stable adduct **5A**, the $Th\cdots H-C_{sp^3}$ distance is 3.299 Å, which is significantly shorter (by ~0.5 Å) than the $Th\cdots H-C_{sp^2}$ distance of 3.736 Å. In contrast, for **6A** the $U\cdots H-C_{sp^2}$ and $U\cdots H-C_{sp^3}$ distances are about the same at 3.455 and 3.401 Å, respectively. This might be an indicator that the H atom on the 2-picoline methyl group for sp^3 activation is more easily accessed in the thorium system to produce the kinetic product, while uranium system does not.

The energies of the four possible adducts for both thorium and uranium are summarized in Table 3. The bent metallocene configurations (**5A**−**C**, **6A**−**C**) are more favorable than the parallel or linear metallocene configuration (**5D** and **6D**).

Complexes **5D** and **6D** are the most unstable adducts with large positive binding energies, which are 4.7 and 10.9 kcal/mol higher in energy, respectively, than the most stable adducts **5A** and **6A**. In comparison, the formation of adducts **5B**, **5C**, **6B**, and **6C** shows small positive reaction energies (<1.50 kcal/mol). Since the difference between **5B**, **5C**, **6B**, and **6C** is merely due to the orientation of the 2-picoline ring, the steric interactions do not have any significant effects on the formation of these adducts.

Attempts to find stable adducts for the C_5Me_5 systems were not successful. Although local minima might not exist, one would expect that the configuration along the reaction pathways of the two reactant molecules ($(C_5Me_5)_2An(CH_3)_2$ and 2-picoline) would closely resemble structures of the adducts calculated for the pathways involving the model C_5H_5 ligand.

Transition States and Reaction Pathways Involved in the C−H Activation Chemistry. As the deuterium labeling studies suggested that the 2-picoline C−H activation chemistry proceeded by σ-bond metathesis for both the thorium and uranium $(C_5Me_5)_2An(CH_3)_2$ complexes,[8] we examined the role of the actinide metal center in the hydrogen atom migration. A search for transition states was carried out for both sp^2 and sp^3 C−H bond activation pathways starting from each adduct to verify if the proposed σ-bond metathesis mechanism was operative. In the discussion that follows, TS refers to the transition state and the subscript refers to the reactant and product. For example, $\mathbf{TS_{5A\text{-}1A}}$ represents the transition state that occurs along the sp^2 C−H bond activation pathway starting from adduct **5A** and giving product **1A**.

Transition States. Figures 7 and 8 show the transition state structures involved in the sp^2 and sp^3 C−H bond activation of 2-picoline from the most stable adduct structures for thorium (**5A**) and uranium (**6A**), respectively. The geometric data for both systems are listed in Table 5. The most important and common characteristic for these transition states are the agostic structures whereby the actinide center mediates the migration of the activated H atom from 2-picoline to leaving methyl group.

For the thorium sp^2 and sp^3 C−H bond activation chemistry, the $Th\cdots H{-}C_{sp^2}$ and $Th\cdots H{-}C_{sp^3}$ Th−H distances are 2.328 and 2.352 Å, respectively. This can be compared with the Th−H bond length of 2.116 Å determined for the model complex $(C_5Me_5)_2Th(H)(CH_3)$. This indicates that a significant bonding interaction exists between the thorium metal center and the migrating H atom. As illustrated in Figure 7, the H atom is not completely transferred from the carbon atom to the thorium atom and the activated carbon−hydrogen bonds are significantly lengthened in all the transition states. In the sp^2 C−H bond activation reaction profile, the bond distance between the thorium metal center and the carbon atom of the leaving methyl group ($Th{-}C^5$) is strongly deformed from 2.538 Å in the adduct **5A** to greater than 2.77 Å in the transition state ($\mathbf{TS_{5A\text{-}1A}}$). In $\mathbf{TS_{5A\text{-}1A}}$, the H atom is also slightly closer to the 2-picoline ($H\cdots C_{sp^2} = 1.340$ Å) than to the leaving Th-methyl group ($H\cdots C_{sp^3} = 1.517$ Å) (Figure 7). To compare, in the thorium-mediated sp^3 C−H bond activation chemistry, the calculated transition state $\mathbf{TS_{5A\text{-}2A}}$ shows that the H atom is approximately located equally between the 2-picoline methyl carbon ($H\cdots C_{sp^3} = 1.431$ Å) and the leaving Th-methyl group ($H\cdots C_{sp^3} = 1.450$ Å).

A similar situation is observed for the uranium system. Starting from **6A**, the lowest energy transition states for both sp^2 and sp^3 C−H bond activation of 2-picoline are the five-member agostic structures, $\mathbf{TS_{6A\text{-}3A}}$ and $\mathbf{TS_{6A\text{-}4A}}$, respectively (Figure 8). The $U\cdots H{-}C_{sp^2}$ and $U\cdots H{-}C_{sp^3}$ U−H distances are 2.247 and 2.258 Å, respectively, in transition states and longer than the U−H bond length in $(C_5Me_5)_2U(H)(CH_3)$, which is 2.044 Å. The migrated H atom sits closer to picoline in the sp^2 transition state and is located at the midpoint of two carbon atoms in the transition state for sp^3 activation. The leaving methyl group binds very weakly with a long coordination bond greater than 2.71 Å.

We refer to this reaction mechanism as "agostic migration", which is a synergistic nonadditive H-migration process. This reaction mechanism is very stereospecific. A similar reaction mechanism has been recently reported for cyclometalation of palladium and iridium.[31,32] These combined data suggest that an "agostic migration mechanism" is operative for the C−H activation in the Th(IV) and U(IV) centers involving a five-center transition state. This differs slightly from the conventional metathesis mechanism, which usually involves a four-center transition state and a H center that does not coordinate with its diagonal atom, in this case the actinide metal center. It has been reported for more than 30 years that agostic structures play an important role in transition metal complexes and catalytic reaction pathways.[33–44] There are only a few reports regarding agostic structures in actinides,[45–49] and practically no mention involving actinide reaction mechanisms.

Reaction Pathways for Thorium and Uranium. The reaction diagram for the sp^2 and sp^3 C−H activation pathways involving the $(C_5H_5)_2Th(CH_3)_2$ complex is shown in Figure 9. In the initial step, the reactants combine to form the weakly bound (1.80 kcal/mol) adduct complex **5A**. Following the sp^3 insertion pathway to form the transition state $\mathbf{TS_{5A\text{-}2A}}$ ($\Delta E^{\ddagger} = 21.46$ kcal/mol), the product **2A** is produced as a kinetic product and product. Along the sp^2 insertion pathway a slightly higher transition state $\mathbf{TS_{5A\text{-}1A}}$ is surmounted ($\Delta E^{\ddagger} = 22.00$ kcal/mol)[50] on the way to formation of the thermodynamic product **1A** (Table 6).

As mentioned earlier, it is unlikely that structures resembling **5B**, **5C**, or **5D** are involved in the reaction pathway, since their energies are 2–4 kcal/mol higher than those of **5A** and also give rise to higher activation energies for C−H insertion. The

(31) Davies, D. L.; Donald, S. M. A.; Macgregor, S. A. *J. Am. Chem. Soc.* **2005**, *127*, 13754–13755.
(32) Davies, D. L.; Donald, S. M. A.; Duaij, O. A.; Macgregor, S. A.; Plleth, M. *J. Am. Chem. Soc.* **2006**, *128*, 4210–4211.
(33) Li, J. L.; Geng, C. Y.; Huang, X. R.; Zhang, X.; Sun, C. C. *Organometallics* **2007**, *26*, 2203–2210.
(34) Brookhart, M.; Green, M. L. H.; Parkin, G. *Proc. Natl. Acad. Sci. U.S.A.* **2007**, *104*, 6908–6914.
(35) Cotton, F. A. *Inorg. Chem.* **2002**, *41*, 643–658.
(36) Paul, A.; Musgrave, C. *Organometallics* **2007**, *26*, 793–809.
(37) Bi, S.; Lin, Z.; Jordan, R. F. *Organometallics* **2004**, *23*, 4882–4890.
(38) Sakaki, S.; Takayama, T.; Sumimoto, M.; Sugimoto, M. *J. Am. Chem. Soc.* **2004**, *126*, 3332–3348.
(39) Ben-Air, E.; Cohen, R.; Gandelman, M.; Shimon, L. J. W.; Martin, J. M. L.; Milstein, D. *Organometallics* **2006**, *25*, 3190–3210.
(40) Niu, S. Q.; Hall, M. B. *Chem. Rev.* **2000**, *100*, 353–405.
(41) Lersch, M.; Tilset, M. *Chem. Rev.* **2005**, *105*, 2471–2526.
(42) Ritleng, V.; Sirlin, C.; Pfeffer, M. *Chem. Rev.* **2002**, *102*, 1731–1769.
(43) Rybtchinski, B.; Cohen, R.; Ben-David, Y.; Martin, J. M. L.; Milstein, D. *J. Am. Chem. Soc.* **2003**, *125*, 11041–11050.
(44) Gilbert, T. M.; Hristov, I.; Ziegler, T. *Organometallics* **2001**, *20*, 1183–1189.
(45) Cruz, C.; Emslie, D.; Harrington, L.; Britten, J.; Robertson, C. *Organometallics* **2007**, *26*, 692–701.
(46) Summerscales, O.; Cloke, F.; Hitchcock, P.; Green, J. C.; Hazari, N. *Science* **2006**, *311*, 829–831.
(47) Andrews, L.; Lyon, J. T. *Inorg. Chem.* **2006**, *45*, 1847–1852.
(48) Clark, D. L.; Grumbine, S. K.; Scott, B. L.; Watkin, J. G. *Organometallics* **1996**, *15*, 949–957.
(49) Barnhart, D.; Clark, D. L.; Grumbine, S. K.; Watkin, J. G. *Inorg. Chem.* **1995**, *34*, 1695–1699.

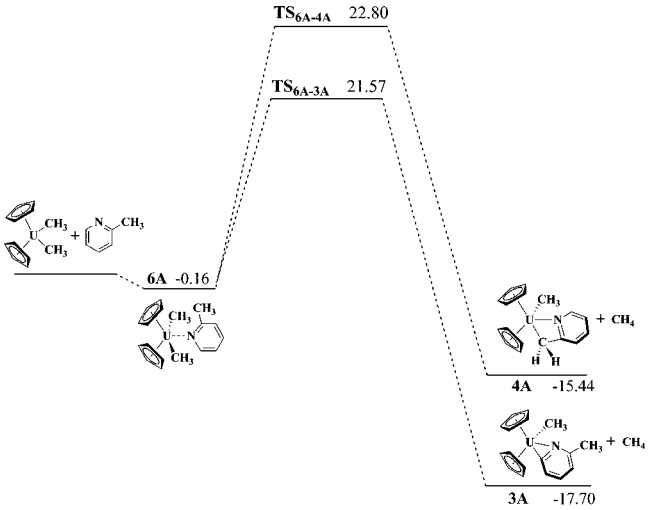

Figure 10. Reaction energy diagram for the sp^2 and sp^3 C−H bond activation chemistry between $(C_5H_5)_2U(CH_3)_2$ and 2-picoline.

transition state structures and reaction energy profile for these species are given in Figure S2 in the Supporting Information.

The calculated reaction pathway for insertion of the adduct **6A** of $(C_5H_5)_2U(CH_3)_2$ into the picoline C−H bonds is illustrated in Figure 10. In contrast to what was found in the thorium reaction, the sp^3 activation (**TS$_{6A-4A}$**) is associated with a higher activation energy than sp^2 activation (**TS$_{6A-3A}$**) by 1.24 kcal/mol. In the case of uranium, the thermodynamically favored product is also the kinetically favored one, leading to the sp^2 product as the only observed product. We also note a larger difference between the sp^2 and sp^3 activation barrier (1.24 kcal/mol) in uranium compared with thorium (0.5 kcal/mol). Despite these small differences, the result is nevertheless consistent with experimental data since no kinetic sp^3 product is observed in the uranium reaction.

The overall results regarding the trends in sp^2 vs sp^3 activation pathways are encouraging in that they delineate the experimental observations to date regarding the difference between Th and U complexes. With respect to the conclusions from previous studies[12,20,21] we first note that these activation energies are calculated for the model C_5H_5 systems. Larger differences might be anticipated between the activation barriers for sp^2 versus sp^3 for C_5Me_5 systems. Indeed we observed larger energy differences between product isomers using C_5Me_5 than with the model C_5H_5 ligand.

We also investigated alternative pathways involving the adducts **6B**, **6C**, and **6D**. These were found to give higher barriers, the same as in the thorium system. The transition state

(50) We have used electronic energies here to examine the reaction pathways. The quantitative results and the trends between Th and U would have been equally well given by the enthalpies at 298 K (see Tables S5 and S6 in the Supporting Information). The Gibbs free energies at 298 K also give consistent predictions as given above with the exception of the relative ordering of the Th sp^2 and sp^3 activation barriers (−1.4 kcal/mol) compared to ZPE corrected energies (+0.7 kcal/mol) The quantities in context use electronic energies without zero-point corrections. Because the low rotation mode of the methyl group on the picoline ring is constrained in the sp^3 activation path, the frequencies of **TS$_{5A-2A}$**(sp^3) are higher than that of **TS$_{5A-1A}$**(sp^2). As a result, the lower entropy contribution of **TS$_{5A-2A}$**(sp^3) leads to a higher Gibbs free energy ($G = H - TS$) compared to **TS$_{5A-1A}$**(sp^2). This observation also holds for the uranium system as well. However, the entropy contributions are calculated for gas-phase species. For reactions in solution, as in the present calculations, the translational, rotational, and low-frequency vibrational contributions to the entropy can be reduced. And as a result, the gas-phase free energies may overestimate the reaction barrier. For a recent discussion, see ref 38.

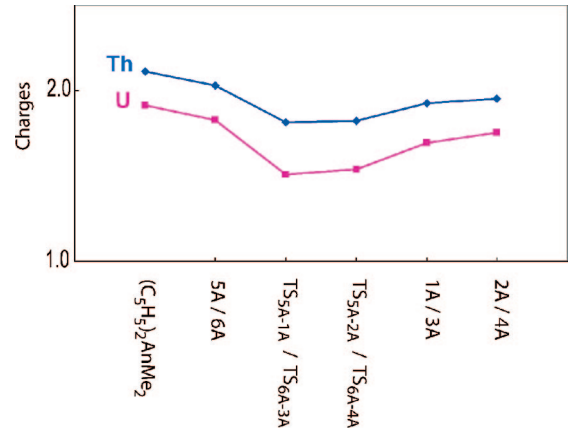

Figure 11. NPA charges on the actinide metal center.

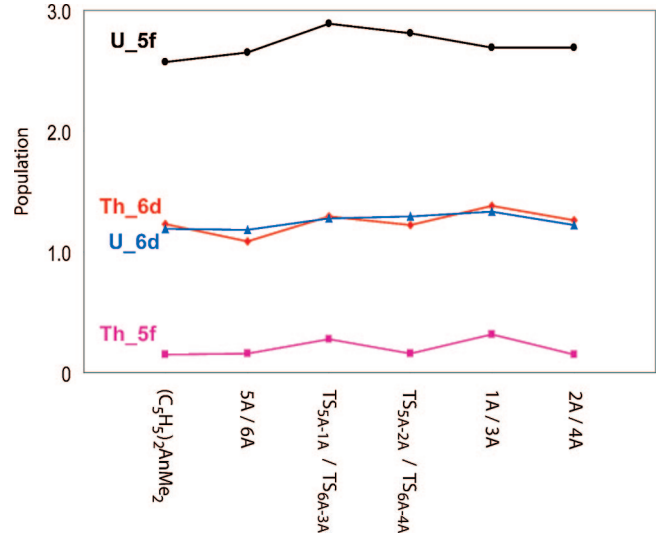

Figure 12. Orbital population on the actinide metal center.

structures and reaction energy profile for these species are given in Figure S3 in the Supporting Information.

Electronic Properties and Solvent Effects. In this section we examine the electronic properties of the reactants, products, and transition states in order to understand the similarities and differences found between the Th and U complexes. Although the differences in thermochemistry and kinetic barriers are consistent with experiment, the differences are subtle involving very small energy changes. We have found no single dominant factor that explains these results.

We begin by discussing the charges determined from the NBO analysis. The NPA charges for the reactants, adducts, transition states, and products for the sp^2 and sp^3 insertion pathways are shown in Figure 11 for both Th and U cases. For Th the natural charges are found to be 2.11, 1.93, and 1.95 respectively for the reactant, the sp^2 product (**1A**), and the sp^3 product (**2A**). As is typically the case, these charges are much smaller than those for the formal +4 oxidation state because of ligand donation of electron density into primarily metal 6d and 5f orbitals. The 6d and 5f populations are depicted in Figure 12 (actual values may be found in Table S4 in the Supporting Information). The thorium 6d populations are 1.29 and 1.38 electrons for the TST and product along the sp^2 pathway and 1.22 and 1.26 electrons for TST and product along the sp^3 pathway. Corresponding values for 5f populations are 0.28 and 0.32 along sp^2 and 0.16 and 0.15 along sp^3 pathways. As seen

in Figure 11, the 6d and 5f populations are slightly higher for the Th complexes along the sp^2 compared to the sp^3 pathway.

For U similar trends can also be seen (Figure 11) in the NPA charge distributions of 1.91, 1.69, and 1.75 in reactant, sp^2 product, and sp^3 product, respectively, resulting in roughly 0.2 higher electron population on the metal center when compared to Th. The U 6d populations are comparable to Th, but with comparable values for both transition states and slightly higher 6d population for the sp^2 product. The higher 5f populations for U reflect the two unpaired electrons in 5f orbitals. After subtracting the population for these two electrons, the remaining 5f populations of approximately 0.7 are higher than the 5f populations of 0.3 in the Th analogues.

As noted earlier, the sp^2 product is more stable than the sp^3 product for both the thorium and uranium systems. From a simply geometric perspective (Figure 2), in the sp^2 product (**1A** and **3A**) the actinide atom is in the picoline ring plane but in the sp^3 product (**2A** and **4A**) it does not lie in the plane. This planar configuration can result in stronger donor−acceptor interactions between the C═N bond on the picolyl ring and the 5f and 6d orbitals on the actinide center. This could account for the fact that the sp^2 product **1A** is the thermodynamically favored pathway.

The possible influence of solvation effects on the reaction mechanisms of Th and U complexes was examined by using the polarizable Continuum Models (PCM).[27,28] One does not anticipate large changes as the reactions were carried out experimentally in the nonpolar solvent toluene with a dielectric constant of 2.38. The solvent effects on the overall reaction thermochemistry and on the reaction barrier were examined. The difference with (and without) solvent effects on thermochemistry for the sp^2 vs sp^3 pathways was 1.6 (1.7) kcal/mol for Th and 3.5 (2.3) kcal/mol for U. The difference between barriers for the sp^2 and sp^3 pathways at their respective transition states was −0.64 (−0.54) kcal/mol for Th and +0.9 (+1.23) kcal/mol for U, and the overall barriers changed by less than 1 kcal/mol. The solvation effects are of the same degree because the complexes along the reaction pathway have similar dipole moments. The solvent-induced dipole moments are about 15% uniformly larger for reactants, adducts, transition states, and products for both Th and U systems. Overall the role of solvent effects does not alter any of the previous conclusions in the previous sections regarding the thermodynamic or kinetic pathways for the C−H insertion reactions.

Conclusions

The current theoretical study provides some insight into the aspects of C−H activation chemistry involving the actinide metal center. The results of density functional theoretical exploration are consistent with reported experimental results. The plausible reaction pathways for the insertion into the sp^2 and sp^3 bonds of $(C_5H_5)_2Th(CH_3)_2$ and $(C_5H_5)_2U(CH_3)_2$, respectively, by 2-picoline are shown in Figures 9 and 10, respectively. In summary, the reaction begins with the formation of a weakly bound or slightly unbound adduct in the case of the model C_5H_5 and the C_5Me_5 complexes, respectively. This is followed by the activation of adjacent C−H bonds by the An-center leading to an agostic transition state. The origin of the regioselectivity rests in the highly ordered nature of the transition states. The calculations find the sp^2-activated structure to be the thermodynamically favored one for both actinide metals. Despite many common features found between thorium and uranium systems, including similar geometries of products, adducts, and the agostic transition states, the relative activation energies between $sp^2$and sp^3 activation differ slightly: Th, $\Delta E^{\ddagger}(sp^2) > \Delta E^{\ddagger}(sp^3)$; U, $\Delta E^{\ddagger}(sp^2) < \Delta E^{\ddagger}(sp^3)$.

These results are in agreement with the experimental observations that the sp^2 insertion product is the thermodynamic product in both cases, but that the sp^3 insertion product is the kinetic product in the case of Th.

The differences in the competition between sp^2 and sp^3 pathways for the two An-centers are subtle. Electronic property analyses confirm that both 5f and 6d orbitals are involved in the product bonding and that oxidative addition is not associated with the reaction process. There does not seem to be a single electronic factor accounting for the differences in reactivity. On the basis of the combination of labeling and structural and computational information, we propose an "agostic migration" cyclomelatation mechanism for C−H activation of N-heterocycles by actinocene complexes.

Acknowledgment. We gratefully thank Jaqueline L. Kiplinger for her helpful discussions and assistance in manuscript publication. This work at Los Alamos National Laboratory was supported by the LANL Glenn T. Seaborg Institute for Transactinium Science (Postdoctoral fellowship to P.Y. and summer research fellowship to I.W.), the LANL Laboratory Directed Research and Development Program, and the Division of Chemical Sciences, Office of Basic Energy Sciences, U.S. Department of Energy under the Heavy Element Chemistry Program at Los Alamos National Laboratory. Los Alamos National Laboratory is operated by Los Alamos National Security, LLC, for the National Nuclear Security Administration of U.S. Department of Energy under contract DE-AC52-06NA25396.

Supporting Information Available: Tables of experimental data obtained from crystal structures and calculated structural data, charge distributions, natural electron configurations, reaction energies, and HOMO-LUMO data, as well as figures showing transition states and reaction energy surfaces. This material is available free of charge via the Internet at http://pubs.acs.org.

OM700927N